Search for $B^0 \to a_0^+(980)\pi^-$

The *BABAR* Collaboration

July 26, 2001

Abstract

We present preliminary results of a search for the decay $B^0 \to a_0^+(980)\pi^-$ among 22.7 million $\Upsilon(4S) \to B\overline{B}$ pairs collected by the *BABAR* detector at PEP-II. Using improved background suppression techniques and optimal signal extraction for rare decay searches, an excess of events over expected background is observed at the level of 3.7 standard deviations. This corresponds to the branching fraction $\mathcal{B}(B^0 \to a_0^+(a_0^+ \to \eta\pi^+)\pi^-) = (6.2^{+3.0}_{-2.5} \pm 1.1) \times 10^{-6}$, where the first error is statistical and the second is systematic. The 90% confidence level upper limit is 11.5×10^{-6}.

The *BABAR* Collaboration,

B. Aubert, D. Boutigny, J.-M. Gaillard, A. Hicheur, Y. Karyotakis, J. P. Lees, P. Robbe, V. Tisserand

Laboratoire de Physique des Particules, F-74941 Annecy-le-Vieux, France

A. Palano

Università di Bari, Dipartimento di Fisica and INFN, I-70126 Bari, Italy

G. P. Chen, J. C. Chen, N. D. Qi, G. Rong, P. Wang, Y. S. Zhu

Institute of High Energy Physics, Beijing 100039, China

G. Eigen, P. L. Reinertsen, B. Stugu

University of Bergen, Inst. of Physics, N-5007 Bergen, Norway

B. Abbott, G. S. Abrams, A. W. Borgland, A. B. Breon, D. N. Brown, J. Button-Shafer, R. N. Cahn,
A. R. Clark, M. S. Gill, A. V. Gritsan, Y. Groysman, R. G. Jacobsen, R. W. Kadel, J. Kadyk, L. T. Kerth,
S. Kluth, Yu. G. Kolomensky, J. F. Kral, C. LeClerc, M. E. Levi, T. Liu, G. Lynch, A. B. Meyer,
M. Momayezi, P. J. Oddone, A. Perazzo, M. Pripstein, N. A. Roe, A. Romosan, M. T. Ronan,
V. G. Shelkov, A. V. Telnov, W. A. Wenzel

Lawrence Berkeley National Laboratory and University of California, Berkeley, CA 94720, USA

P. G. Bright-Thomas, T. J. Harrison, C. M. Hawkes, D. J. Knowles, S. W. O'Neale, R. C. Penny,
A. T. Watson, N. K. Watson

University of Birmingham, Birmingham, B15 2TT, United Kingdom

T. Deppermann, K. Goetzen, H. Koch, J. Krug, M. Kunze, B. Lewandowski, K. Peters, H. Schmuecker,
M. Steinke

Ruhr Universität Bochum, Institut für Experimentalphysik 1, D-44780 Bochum, Germany

J. C. Andress, N. R. Barlow, W. Bhimji, N. Chevalier, P. J. Clark, W. N. Cottingham, N. De Groot,
N. Dyce, B. Foster, J. D. McFall, D. Wallom, F. F. Wilson

University of Bristol, Bristol BS8 1TL, United Kingdom

K. Abe, C. Hearty, T. S. Mattison, J. A. McKenna, D. Thiessen

University of British Columbia, Vancouver, BC, Canada V6T 1Z1

S. Jolly, A. K. McKemey, J. Tinslay

Brunel University, Uxbridge, Middlesex UB8 3PH, United Kingdom

V. E. Blinov, A. D. Bukin, D. A. Bukin, A. R. Buzykaev, V. B. Golubev, V. N. Ivanchenko, A. A. Korol,
E. A. Kravchenko, A. P. Onuchin, A. A. Salnikov, S. I. Serednyakov, Yu. I. Skovpen, V. I. Telnov,
A. N. Yushkov

Budker Institute of Nuclear Physics, Novosibirsk 630090, Russia

D. Best, A. J. Lankford, M. Mandelkern, S. McMahon, D. P. Stoker

University of California at Irvine, Irvine, CA 92697, USA

A. Ahsan, K. Arisaka, C. Buchanan, S. Chun

University of California at Los Angeles, Los Angeles, CA 90024, USA

J. G. Branson, D. B. MacFarlane, S. Prell, Sh. Rahatlou, G. Raven, V. Sharma

University of California at San Diego, La Jolla, CA 92093, USA

C. Campagnari, B. Dahmes, P. A. Hart, N. Kuznetsova, S. L. Levy, O. Long, A. Lu, J. D. Richman,
W. Verkerke, M. Witherell, S. Yellin

University of California at Santa Barbara, Santa Barbara, CA 93106, USA

J. Beringer, D. E. Dorfan, A. M. Eisner, A. Frey, A. A. Grillo, M. Grothe, C. A. Heusch, R. P. Johnson,
W. Kroeger, W. S. Lockman, T. Pulliam, H. Sadrozinski, T. Schalk, R. E. Schmitz, B. A. Schumm,
A. Seiden, M. Turri, W. Walkowiak, D. C. Williams, M. G. Wilson

University of California at Santa Cruz, Institute for Particle Physics, Santa Cruz, CA 95064, USA

E. Chen, G. P. Dubois-Felsmann, A. Dvoretskii, D. G. Hitlin, S. Metzler, J. Oyang, F. C. Porter, A. Ryd,
A. Samuel, M. Weaver, S. Yang, R. Y. Zhu

California Institute of Technology, Pasadena, CA 91125, USA

S. Devmal, T. L. Geld, S. Jayatilleke, G. Mancinelli, B. T. Meadows, M. D. Sokoloff

University of Cincinnati, Cincinnati, OH 45221, USA

T. Barillari, P. Bloom, M. O. Dima, S. Fahey, W. T. Ford, D. R. Johnson, U. Nauenberg, A. Olivas,
H. Park, P. Rankin, J. Roy, S. Sen, J. G. Smith, W. C. van Hoek, D. L. Wagner

University of Colorado, Boulder, CO 80309, USA

J. Blouw, J. L. Harton, M. Krishnamurthy, A. Soffer, W. H. Toki, R. J. Wilson, J. Zhang

Colorado State University, Fort Collins, CO 80523, USA

T. Brandt, J. Brose, T. Colberg, G. Dahlinger, M. Dickopp, R. S. Dubitzky, A. Hauke, E. Maly,
R. Müller-Pfefferkorn, S. Otto, K. R. Schubert, R. Schwierz, B. Spaan, L. Wilden

Technische Universität Dresden, Institut für Kern- und Teilchenphysik, D-01062, Dresden, Germany

L. Behr, D. Bernard, G. R. Bonneaud, F. Brochard, J. Cohen-Tanugi, S. Ferrag, E. Roussot, S. T'Jampens,
Ch. Thiebaux, G. Vasileiadis, M. Verderi

Ecole Polytechnique, F-91128 Palaiseau, France

A. Anjomshoaa, R. Bernet, A. Khan, D. Lavin, F. Muheim, S. Playfer, J. E. Swain

University of Edinburgh, Edinburgh EH9 3JZ, United Kingdom

M. Falbo

Elon University, Elon University, NC 27244-2010, USA

C. Borean, C. Bozzi, S. Dittongo, M. Folegani, L. Piemontese

Università di Ferrara, Dipartimento di Fisica and INFN, I-44100 Ferrara, Italy

E. Treadwell

Florida A&M University, Tallahassee, FL 32307, USA

F. Anulli,[1] R. Baldini-Ferroli, A. Calcaterra, R. de Sangro, D. Falciai, G. Finocchiaro, P. Patteri,
I. M. Peruzzi,[2][1] M. Piccolo, Y. Xie, A. Zallo

Laboratori Nazionali di Frascati dell'INFN, I-00044 Frascati, Italy

---

[1]Also with Università di Perugia, I-06100 Perugia, Italy

S. Bagnasco, A. Buzzo, R. Contri, G. Crosetti, P. Fabbricatore, S. Farinon, M. Lo Vetere, M. Macri,
M. R. Monge, R. Musenich, M. Pallavicini, R. Parodi, S. Passaggio, F. C. Pastore, C. Patrignani,
M. G. Pia, C. Priano, E. Robutti, A. Santroni

Università di Genova, Dipartimento di Fisica and INFN, I-16146 Genova, Italy

M. Morii

Harvard University, Cambridge, MA 02138, USA

R. Bartoldus, T. Dignan, R. Hamilton, U. Mallik

University of Iowa, Iowa City, IA 52242, USA

J. Cochran, H. B. Crawley, P.-A. Fischer, J. Lamsa, W. T. Meyer, E. I. Rosenberg

Iowa State University, Ames, IA 50011-3160, USA

M. Benkebil, G. Grosdidier, C. Hast, A. Höcker, H. M. Lacker, S. Laplace, V. Lepeltier, A. M. Lutz,
S. Plaszczynski, M. H. Schune, S. Trincaz-Duvoid, A. Valassi, G. Wormser

Laboratoire de l'Accélérateur Linéaire, F-91898 Orsay, France

R. M. Bionta, V. Brigljević , D. J. Lange, M. Mugge, X. Shi, K. van Bibber, T. J. Wenaus, D. M. Wright,
C. R. Wuest

Lawrence Livermore National Laboratory, Livermore, CA 94550, USA

M. Carroll, J. R. Fry, E. Gabathuler, R. Gamet, M. George, M. Kay, D. J. Payne, R. J. Sloane,
C. Touramanis

University of Liverpool, Liverpool L69 3BX, United Kingdom

M. L. Aspinwall, D. A. Bowerman, P. D. Dauncey, U. Egede, I. Eschrich, N. J. W. Gunawardane,
J. A. Nash, P. Sanders, D. Smith

University of London, Imperial College, London, SW7 2BW, United Kingdom

D. E. Azzopardi, J. J. Back, P. Dixon, P. F. Harrison, R. J. L. Potter, H. W. Shorthouse, P. Strother,
P. B. Vidal, M. I. Williams

Queen Mary, University of London, E1 4NS, United Kingdom

G. Cowan, S. George, M. G. Green, A. Kurup, C. E. Marker, P. McGrath, T. R. McMahon, S. Ricciardi,
F. Salvatore, I. Scott, G. Vaitsas

*University of London, Royal Holloway and Bedford New College, Egham, Surrey TW20 0EX, United
Kingdom*

D. Brown, C. L. Davis

University of Louisville, Louisville, KY 40292, USA

J. Allison, R. J. Barlow, J. T. Boyd, A. C. Forti, J. Fullwood, F. Jackson, G. D. Lafferty, N. Savvas,
E. T. Simopoulos, J. H. Weatherall

University of Manchester, Manchester M13 9PL, United Kingdom

A. Farbin, A. Jawahery, V. Lillard, J. Olsen, D. A. Roberts, J. R. Schieck

University of Maryland, College Park, MD 20742, USA

G. Blaylock, C. Dallapiccola, K. T. Flood, S. S. Hertzbach, R. Kofler, T. B. Moore, H. Staengle, S. Willocq

University of Massachusetts, Amherst, MA 01003, USA

4

B. Brau, R. Cowan, G. Sciolla, F. Taylor, R. K. Yamamoto

Massachusetts Institute of Technology, Laboratory for Nuclear Science, Cambridge, MA 02139, USA

M. Milek, P. M. Patel, J. Trischuk

McGill University, Montréal, Canada QC H3A 2T8

F. Lanni, F. Palombo

Università di Milano, Dipartimento di Fisica and INFN, I-20133 Milano, Italy

J. M. Bauer, M. Booke, L. Cremaldi, V. Eschenburg, R. Kroeger, J. Reidy, D. A. Sanders, D. J. Summers

University of Mississippi, University, MS 38677, USA

J. P. Martin, J. Y. Nief, R. Seitz, P. Taras, A. Woch, V. Zacek

Université de Montréal, Laboratoire René J. A. Lévesque, Montréal, Canada QC H3C 3J7

H. Nicholson, C. S. Sutton

Mount Holyoke College, South Hadley, MA 01075, USA

C. Cartaro, N. Cavallo,[3] G. De Nardo, F. Fabozzi, C. Gatto, L. Lista, P. Paolucci, D. Piccolo, C. Sciacca

Università di Napoli Federico II, Dipartimento di Scienze Fisiche and INFN, I-80126, Napoli, Italy

J. M. LoSecco

University of Notre Dame, Notre Dame, IN 46556, USA

J. R. G. Alsmiller, T. A. Gabriel, T. Handler

Oak Ridge National Laboratory, Oak Ridge, TN 37831, USA

J. Brau, R. Frey, M. Iwasaki, N. B. Sinev, D. Strom

University of Oregon, Eugene, OR 97403, USA

F. Colecchia, F. Dal Corso, A. Dorigo, F. Galeazzi, M. Margoni, G. Michelon, M. Morandin, M. Posocco, M. Rotondo, F. Simonetto, R. Stroili, E. Torassa, C. Voci

Università di Padova, Dipartimento di Fisica and INFN, I-35131 Padova, Italy

M. Benayoun, H. Briand, J. Chauveau, P. David, Ch. de la Vaissière, L. Del Buono, O. Hamon, F. Le Diberder, Ph. Leruste, J. Lory, L. Roos, J. Stark, S. Versillé

Universités Paris VI et VII, Lab de Physique Nucléaire H. E., F-75252 Paris, France

P. F. Manfredi, V. Re, V. Speziali

Università di Pavia, Dipartimento di Elettronica and INFN, I-27100 Pavia, Italy

E. D. Frank, L. Gladney, Q. H. Guo, J. H. Panetta

University of Pennsylvania, Philadelphia, PA 19104, USA

C. Angelini, G. Batignani, S. Bettarini, M. Bondioli, M. Carpinelli, F. Forti, M. A. Giorgi, A. Lusiani, F. Martinez-Vidal, M. Morganti, N. Neri, E. Paoloni, M. Rama, G. Rizzo, F. Sandrelli, G. Simi, G. Triggiani, J. Walsh

Università di Pisa, Scuola Normale Superiore and INFN, I-56010 Pisa, Italy

---

[3]Also with Università della Basilicata, I-85100 Potenza, Italy

M. Haire, D. Judd, K. Paick, L. Turnbull, D. E. Wagoner

Prairie View A&M University, Prairie View, TX 77446, USA

J. Albert, C. Bula, P. Elmer, C. Lu, K. T. McDonald, V. Miftakov, S. F. Schaffner, A. J. S. Smith,
A. Tumanov, E. W. Varnes

Princeton University, Princeton, NJ 08544, USA

G. Cavoto, D. del Re, R. Faccini,[4] F. Ferrarotto, F. Ferroni, K. Fratini, E. Lamanna, E. Leonardi,
M. A. Mazzoni, S. Morganti, G. Piredda, F. Safai Tehrani, M. Serra, C. Voena

Università di Roma La Sapienza, Dipartimento di Fisica and INFN, I-00185 Roma, Italy

S. Christ, R. Waldi

Universität Rostock, D-18051 Rostock, Germany

P. F. Jacques, M. Kalelkar, R. J. Plano

Rutgers University, New Brunswick, NJ 08903, USA

T. Adye, B. Franek, N. I. Geddes, G. P. Gopal, S. M. Xella

Rutherford Appleton Laboratory, Chilton, Didcot, Oxon, OX11 0QX, United Kingdom

R. Aleksan, G. De Domenico, S. Emery, A. Gaidot, S. F. Ganzhur, P.-F. Giraud, G. Hamel de
Monchenault, W. Kozanecki, M. Langer, G. W. London, B. Mayer, B. Serfass, G. Vasseur, Ch. Yèche,
M. Zito

DAPNIA, Commissariat à l'Energie Atomique/Saclay, F-91191 Gif-sur-Yvette, France

N. Copty, M. V. Purohit, H. Singh, F. X. Yumiceva

University of South Carolina, Columbia, SC 29208, USA

I. Adam, P. L. Anthony, D. Aston, K. Baird, J. P. Berger, E. Bloom, A. M. Boyarski, F. Bulos,
G. Calderini, R. Claus, M. R. Convery, D. P. Coupal, D. H. Coward, J. Dorfan, M. Doser, W. Dunwoodie,
R. C. Field, T. Glanzman, G. L. Godfrey, S. J. Gowdy, P. Grosso, T. Himel, T. Hryn'ova, M. E. Huffer,
W. R. Innes, C. P. Jessop, M. H. Kelsey, P. Kim, M. L. Kocian, U. Langenegger, D. W. G. S. Leith,
S. Luitz, V. Luth, H. L. Lynch, H. Marsiske, S. Menke, R. Messner, K. C. Moffeit, R. Mount, D. R. Muller,
C. P. O'Grady, M. Perl, S. Petrak, H. Quinn, B. N. Ratcliff, S. H. Robertson, L. S. Rochester,
A. Roodman, T. Schietinger, R. H. Schindler, J. Schwiening, V. V. Serbo, A. Snyder, A. Soha,
S. M. Spanier, J. Stelzer, D. Su, M. K. Sullivan, H. A. Tanaka, J. Va'vra, S. R. Wagner,
A. J. R. Weinstein, W. J. Wisniewski, D. H. Wright, C. C. Young

Stanford Linear Accelerator Center, Stanford, CA 94309, USA

P. R. Burchat, C. H. Cheng, D. Kirkby, T. I. Meyer, C. Roat

Stanford University, Stanford, CA 94305-4060, USA

R. Henderson

TRIUMF, Vancouver, BC, Canada V6T 2A3

W. Bugg, H. Cohn, A. W. Weidemann

University of Tennessee, Knoxville, TN 37996, USA

---

[4]Also with University of California at San Diego, La Jolla, CA 92093, USA

J. M. Izen, I. Kitayama, X. C. Lou, M. Turcotte

University of Texas at Dallas, Richardson, TX 75083, USA

F. Bianchi, M. Bona, B. Di Girolamo, D. Gamba, A. Smol, D. Zanin

Università di Torino, Dipartimento di Fisica Sperimentale and INFN, I-10125 Torino, Italy

L. Bosisio, G. Della Ricca, L. Lanceri, A. Pompili, P. Poropat, M. Prest, E. Vallazza, G. Vuagnin

Università di Trieste, Dipartimento di Fisica and INFN, I-34127 Trieste, Italy

R. S. Panvini

Vanderbilt University, Nashville, TN 37235, USA

C. M. Brown, A. De Silva, R. Kowalewski, J. M. Roney

University of Victoria, Victoria, BC, Canada V8W 3P6

H. R. Band, E. Charles, S. Dasu, F. Di Lodovico, A. M. Eichenbaum, H. Hu, J. R. Johnson, R. Liu,
J. Nielsen, Y. Pan, R. Prepost, I. J. Scott, S. J. Sekula, J. H. von Wimmersperg-Toeller, S. L. Wu, Z. Yu,
H. Zobernig

University of Wisconsin, Madison, WI 53706, USA

T. M. B. Kordich, H. Neal

Yale University, New Haven, CT 06511, USA

1 Introduction

We present a search for the decay $B^0 \to a_0^+(980)\pi^-$, where the a_0 resonance[1] is observed in its dominant decay channel $a_0^+ \to \eta\pi^+$. The interest in this mode stems from its potential use for measuring the CKM angle α [1, 2]. It was pointed out in Ref. [2] that, within the factorization assumption, the main tree contributions to the $a_0\pi$ decay amplitude vanish: they would imply forbidden second class currents. This simplifies the two-body analysis for the extraction of α, and can lead to an enhanced direct CP violation.

After a preselection, we refine the background suppression using Multivariate Analyzer (MVA) tools (Neural Net (NN) and Fisher discriminants). We use both cut-based and shape-based analyses, the latter employing a maximum likelihood technique, which together provide complementary results and cross-checks. The cut optimization procedure used in the analysis does not rely on a prior branching fraction estimate. Both inclusive and exclusive control samples are used for systematics checks, particularly with regard to the η and a_0 resonances [3].

2 The *BABAR* Detector and the Dataset

The data used in this analysis were collected with the *BABAR* detector at the PEP-II storage ring, located at the Stanford Linear Accelerator Center (SLAC). PEP-II is an asymmetric e^+e^- collider with a center-of-mass energy equal to the $\Upsilon(4S)$ mass. From Nov. 1999 to Oct. 2000, a total of 22.7 million $B\overline{B}$ pairs has been collected by *BABAR*, corresponding to an integrated on-peak luminosity of approximately $20.7\,\mathrm{fb}^{-1}$. In addition, $2.6\,\mathrm{fb}^{-1}$ of off-peak data were taken during the same period: they have been used to validate the contribution to backgrounds resulting from e^+e^- annihilation into light $q\overline{q}$ pairs.

The *BABAR* detector and its performance are described in Ref. [4]. The innermost component consists of a 5-layer Silicon Vertex Tracker (SVT), providing the positions of charged tracks in the neighbourhood of the beam interaction point. It is followed by a 40-layer central Drift Chamber (DCH), immersed in a 1.5-T magnetic field, measuring the track momenta and providing a measurement of the specific ionization loss ($\mathrm{d}E/\mathrm{d}x$) for particle identification (PID). The main PID device is a unique, internally reflecting ring imaging Cherenkov detector (DIRC), covering the central region of *BABAR*. A Cherenkov angle K/π separation of better than 4 standard deviations is achieved for tracks below $3\,\mathrm{GeV}/c$ momentum. Photons are detected by a CsI(Tl) electromagnetic calorimeter (EMC), which provides excellent angular and energy resolution with high efficiency for energy deposits above $20\,\mathrm{MeV}$. A superconducting solenoid, located around the EMC is itself surrounded by an iron flux return, instrumented with Resistive Plate Chambers to identify muons.

3 Analysis Method

3.1 Candidate Selection

A $B^0 \to a_0^+\pi^-$ candidate contains a pair of oppositely-charged pions and two photons. Charged tracks are required to satisfy a set of track quality criteria, which includes cuts on their momenta (less than $10\,\mathrm{GeV}/c$), transverse momenta (above $100\,\mathrm{MeV}/c$), and on the number of DCH hits (at least 20). The tracks are also required to originate in the vicinity of the beam-beam interaction point. Pion candidates must fail electron selection criteria and are required to have a momentum

---

[1]Charge conjugation is implied throughout this document, and the $a_0^+(980)$ resonance is denoted a_0.

in the center-of-mass (CM) above $2\,\text{GeV}/c$. A B candidate is rejected if the track not used to form the a_0 has a DIRC Cherenkov angle consistent with a kaon. Photons are identified as energy deposits in the EMC, unassociated with charged tracks. They are required to have an energy above $80\,\text{MeV}$ in the laboratory frame (LAB), and must satisfy photon-like shower profile criteria. To be associated with an η decay, a pair of candidate photons is required to have an invariant mass $0.470 < m(\gamma\gamma) < 0.615\,\text{GeV}/c^2$, and the η CM momentum must be larger than $0.9\,\text{GeV}/c$. The pion track and η candidate form an a_0 candidate if their invariant mass falls in the range $0.9 < m(\eta\pi) < 1.08\,\text{GeV}/c^2$. Reconstruction of B^0 candidates is done by vertexing all combinations of $\pi^+\pi^-\eta$ candidates in each event and applying a quality requirement on the $\pi^+\pi^-$ vertex. A B^0 candidate is characterized by two kinematic variables: the beam energy-constrained mass $m_{\text{EC}} = \sqrt{E_{\text{beam}}^2 - p_B^2}$, where E_{beam} is half the CM energy and p_B is obtained by applying kinematic constraints to the four-momenta of the B daughters; and $|\Delta E| \equiv |E_B - E_{\text{beam}}|$ with E_B being the CM energy of the B candidate. A candidate is retained if $m_{\text{EC}} > 5.21\,\text{GeV}/c^2$ and $|\Delta E| < 0.25\,\text{GeV}$.

3.2   Background Suppression

Charmless hadronic modes suffer from large amounts of background from random combinations of tracks, mostly from light quark production. In the CM frame, this background typically exhibits a two-jet structure in contrast to the spherically symmetric $\Upsilon(4S) \to B\overline{B}$ events. Efficient background rejection is obtained by requiring the angle θ_{T} between the thrust axis of the B candidate and the thrust axis of the rest of the event (ROE) to satisfy $|\cos\theta_{\text{T}}| < 0.9$. Denoting $|\cos\theta_{\text{TP}}|$ as the minimum cosine of the two angles formed by the two most energetic tracks (or neutral clusters) with respect to the thrust axis of the event, we require $|\cos\theta_{\text{TP}}| < 0.88$. Combinatorial background within a candidate event arises mainly from low-energy photons. Compared with decay modes containing π^0's, this is a minor concern for $a_0\pi$ due to the higher η mass: the fraction of events with more than one photon pair combination passing the selection cuts is at the percent level. For events with multiple candidates the one with the most energetic low-energy photon is retained.

Further discrimination is achieved by combining event shape variables using MVA techniques. A common approach uses the Fisher discriminant (denoted *standard Fisher* below) proposed by the CLEO Collaboration [7]. This standard Fisher is built as a linear combination of the cosine of the angle between the B candidate momentum and the beam axis, the cosine of the angle between the B candidate thrust axis and the beam axis, together with nine energy deposits, each defined to be the energy of charged tracks and neutral clusters of the ROE whose directions are contained in nine concentric cones centered around the B direction. In our analysis, the choice of variables has been reconsidered taking into account the separation power[2], the correlations between the variables and the signal efficiency at fixed background rejection. For this purpose, 12 variables are selected and combined using either a linear (Fisher) or a non-linear (NN) MVA. Table 1 lists the variables which are retained together with their respective Fisher coefficients. Among thse are the six variables

---

[2]The separation power of the normalized signal and background distributions, $S(x)$ and $B(x)$, of a discriminating variable x, is defined by

$$\langle s^2 \rangle = \frac{1}{2} \int\limits_{-\infty}^{+\infty} dx \frac{(S(x) - B(x))^2}{S(x) + B(x)} \ .$$
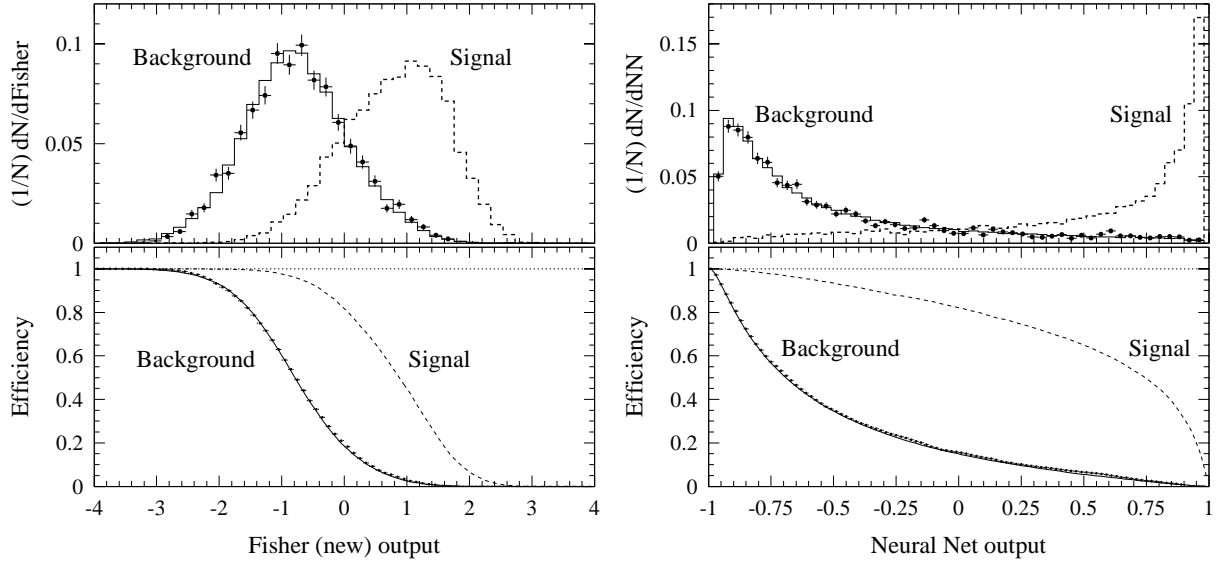
Figure 1: Fisher (left-hand plots) and Neural Net discriminants (right-hand plots). The upper plots show the distributions for signal and background, where the signal is taken from Monte Carlo simulation and the background from on-peak sideband data. The points with error bars show the off-peak data, containing no signal. The lower plots show the signal and background efficiencies as a function of the cut applied (the small dots indicate the off-peak data).

$L_j^{(c)}$, $L_j^{(n)}$ $(j = 0, 2, 6)$ defined by

$$L_j^{(c,n)} = \sum_{i_{(c,n)}} p_i \times |\cos\theta_i|^j \; , \tag{1}$$

which are the momentum-weighted sums of the cosines of the angles between the ROE charged tracks $(L_j^{(c)})$ or neutral clusters $(L_j^{(n)})$ and the thrust axis of the B candidate. These variables provide a generalization of the discrete cones used in the standard Fisher discriminant.

Figure 1 shows the distributions of the Fisher and NN discriminants for signal and background, the former taken from Monte Carlo simulation and the latter from on-peak sideband data (histograms) and from off-peak data (points with error bars). The lower plots show the resulting signal and background efficiencies as a function of a cut applied on the output values of the discriminants. Figure 2 depicts the background versus signal efficiencies for the standard Fisher discriminant and the 12-variable MVAs adopted in this analysis. A 17% relative increase of the signal efficiency is obtained for NN with respect to the standard Fisher at the benchmark of 5% background retention. Table 2 summarizes the performances of the three MVA discriminants. The NN, being the discriminant which provides the best signal efficiency, is used for the signal extraction in this analysis, while keeping the Fisher for cross-checks.
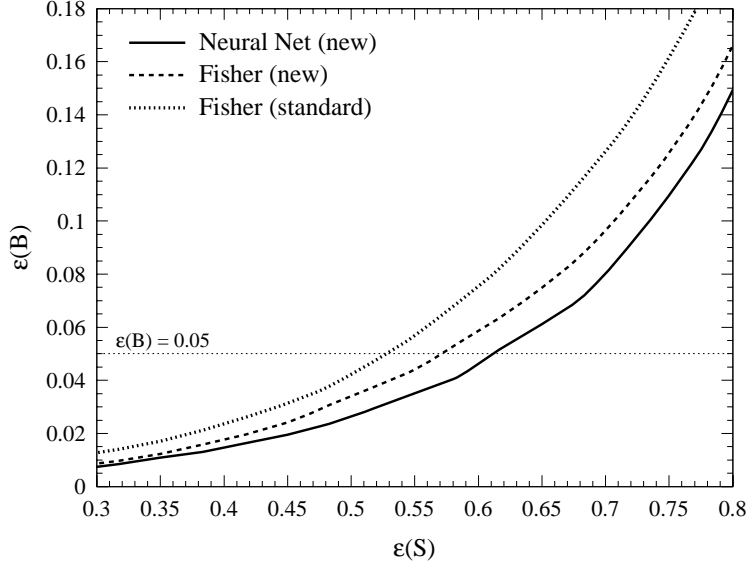
10

Figure 2: Comparison of the background versus signal efficiencies for NN (solid line), the Fisher (dashed line), and the standard Fisher (dashed-dotted line) discriminants.

3.3 Cut-Based Analysis

The signal extraction is based on counting data events found in a signal region (SR) and subtracting from this the expected background yield. To find an optimal set of signal selection criteria, balancing between background rejection and signal efficiency, we use the procedure described in the appendix. The criterion it applies is to minimize the expected confidence level for the null hypothesis "there is no signal in the data sample". Cut optimization is performed on the MVA output only, resulting in the requirements $x_{\mathrm{opt}}^{\mathrm{out}}(\mathrm{NN}) > 0.6$ and $x_{\mathrm{opt}}^{\mathrm{out}}(\mathrm{Fisher}) > 0.7$, respectively.

The SR is defined as $|m_{\mathrm{EC}} - 5.28| < 0.006 \, \mathrm{GeV}/c^2$, $|\Delta E| < 0.070 \, \mathrm{GeV}$ and $0.517 < m(\gamma\gamma) < 0.587 \, \mathrm{GeV}/c^2$. The background contamination in the SR is estimated from the two-dimensional Grand Sideband (GSB): $|\Delta E| < 0.25 \, \mathrm{GeV}$ and $5.210 < m_{\mathrm{EC}} < 5.263 \, \mathrm{GeV}/c^2$, assuming for the corresponding background shapes a second-order polynomial for ΔE, and an ARGUS function [8] for m_{EC}. The signal efficiencies (ϵ), event yields ($\mathcal{N}$) and the expected backgrounds (N_b) are given in Table 3 for Fisher and NN. The corresponding branching fractions are obtained from the expression

$$\mathcal{B} = \frac{\mathcal{N} - N_b}{\epsilon \, N_{B\bar{B}}} \, , \tag{2}$$

where $N_{B\bar{B}} = (22.74 \pm 0.36) \times 10^6$ is the total number of produced $B\bar{B}$ pairs. Equation 2 assumes an equal production of charged and neutral B's in $\Upsilon(4S)$ decays. Non-resonant contributions to the $\eta\pi^+\pi^-$ final state are disregarded for all branching fractions quoted in this document. The results obtained using Fisher and NN are compatible. Their statistical significances, defined as the probability to observe the given excess when no signal is present, are 3.0 and 3.1 standard deviations, respectively. The systematic errors assigned to the branching fractions are described in Sec. 4. Also given in Table 3 are the upper limits at 90% confidence levels, where the systematic

11

Table 1: The 12 event-shape variables used as MVA inputs with their corresponding Fisher coefficients.

Variable name	Description	Fisher coefficient
R_2	Second Fox-Wolfram moment	0.40
$|\cos\theta_{\mathrm{T}}|$	Angle: B/ROE thrust axis	-0.71
$|\cos\theta_{\mathrm{S}}|$	Angle: B/ROE sphericity axis	-0.89
$|\cos(B, z)|$	Angle: B direction/beam axis	-0.88
$|\cos(B(\mathrm{T}), z)|$	Angle: B thrust/beam axis	-0.79
$|\cos\theta_{\mathrm{TP}}|$	Minimum cosine of ROE tracks/clusters	0.54
L_0^{n}	Neutral zeroth-order angular function	0.35
L_2^{n}	Neutral second-order angular function	-1.02
L_6^{n}	Neutral sixth-order angular function	-0.69
L_0^{c}	Charged zeroth-order angular function	0.38
L_2^{c}	Charged second-order angular function	-0.51
L_6^{c}	Charged sixth order angular function	-0.66
Offset	*Centers the sum of signal and background at zero*	1.49

Table 2: Results on the separation and the signal efficiency at the benchmark of 5% background retention for the standard Fisher discriminant and the two MVAs used in this analysis.

Type	$\langle s^2 \rangle$	$\epsilon(S)$(at $\epsilon(B) = 5\%$)
Fisher (standard)	0.44	0.52
Fisher (12-var.)	0.48	0.57
Neural Net (12-var.)	0.50	0.61

errors are added linearly to the statistical limits.

The m_{EC} distribution of the events passing the selection requirements (except for the m_{EC} cut) is shown in Fig. 3 (for NN). For illustration purposes, we have superimposed the Gaussian signal contribution and the ARGUS background contribution; both distributions are normalized to the results given in Table 3.

3.4 Maximum Likelihood Analysis

The likelihood $P(f, x_i)$ for event $\{i\}$ with a measured set of discriminating variables x_i, and for a signal fraction f, is defined as

$$P(f, x_i) = f p_s(x_i) + (1 - f) p_b(x_i) \ . \tag{3}$$

The $p_s(x_i)$ ($p_b(x_i)$) is the product of the normalized signal (background) probability density functions (PDF) of the individual variables entering the fit: namely, m_{EC}, ΔE, $m(\eta)$ and the NN or Fisher output. The $\eta\pi$ invariant mass is not included since the line shape of the a_0 resonance is not

Table 3: Selection efficiencies, expected signal and background yields for the cut-based analysis using Fisher or NN. When two errors are given, the first is statistical and the second is systematic. We quote upper limits as the main results and compute branching fractions and statistical significances, should the observed excess be interpreted as evidence for a signal. The systematic errors are discussed in Sec. 4.

	Fisher	Neural Net
Signal efficiency (%)	14.2	14.6
Events in signal box	20	18
Events in GSB	242	197
Expected background events in signal box	$9.6 \pm 0.6 \pm 1.4$	$7.9 \pm 0.6 \pm 1.1$
Branching fraction ($\times 10^{-6}$)	$8.2^{+4.6}_{-3.0} \pm 1.4$	$7.8^{+4.0}_{-2.7} \pm 1.2$
Statistical significance	3.0σ	3.1σ
90% CL Upper limit ($\times 10^{-6}$)	15.3	14.5
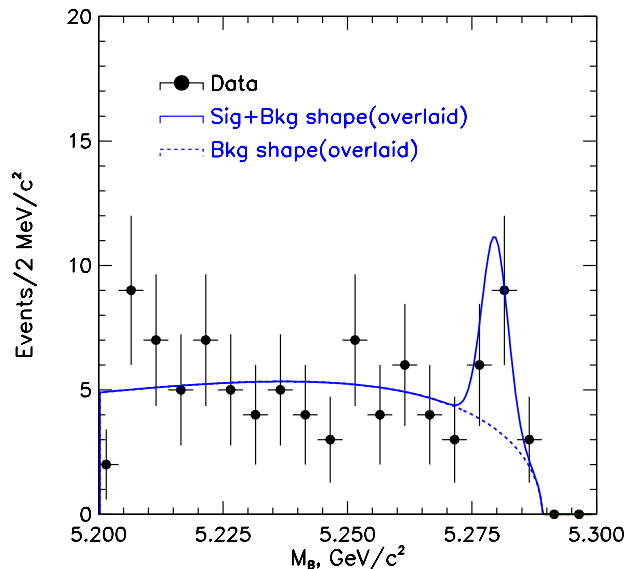
Figure 3: Distribution of m_{EC} obtained from the cut-based analysis using the NN. Superimposed on the data points are the signal and background m_{EC} distributions, normalized to the number of observed events.

well known at present [3]. The data sample is selected within generous sidebands for the variables that enter the fit (*c.f.* Sec. 3.1). The signal distributions are obtained from Monte Carlo simulation, refined with data from the signal-like charmed B decay mode $D\rho$, and inclusive samples. On-peak sideband events, controlled by off-peak data, are used to infer the corresponding background shapes. Multi-Gaussian, polynomial functions and cubic splines have been used to empirically approximate
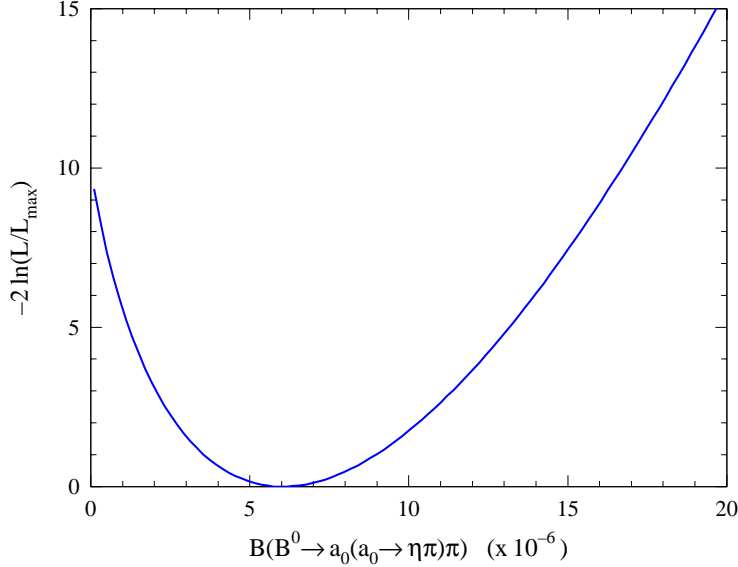
Figure 4: Negative log-likelihood function versus the signal branching fraction.

the reconstructed shapes of the discriminating variables.

After applying the event selection described in Sec. 3.1, a total of $\mathcal{N} = 9248$ candidate events without multiple combinations enters the ML fit, corresponding to a signal efficiency of 32.8%. The fit is performed by minimizing the sum

$$-2\ln\mathcal{L}_f = -2\sum_{i=1}^{\mathcal{N}} \ln P(f, x_i) \ , \tag{4}$$

over $\mathcal{N}$ events, with respect to the signal fraction f. The fit results in $N_s = f\mathcal{N} = 18.1\,^{+8.7}_{-7.4}$ signal events for NN, and $N_s = 16.2\,^{+8.6}_{-7.2}$ signal events for Fisher[3]. In the following, we restrict the discussion to the results obtained with the NN, since it provides the best signal efficiency. This choice has been made prior to uncovering the results. The negative log-likelihood function versus the signal branching fraction is depicted in Fig. 4. A "toy" Monte Carlo simulation indicates a goodness-of-fit of 50%. If the observed signal excess is interpreted as evidence for a signal, the corresponding branching fraction is

$$\mathcal{B}(B^0 \to a_0^{\pm}(a_0^{\pm} \to \eta\pi^{\pm})\pi^{\mp}) = (6.2\,^{+3.0}_{-2.5} \pm 1.1) \times 10^{-6} \ , \tag{5}$$

where the first error quoted is statistical and the second is systematic. The statistical significance of this result corresponds to 3.7 standard deviations. The latter is computed using a zero-signal toy Monte Carlo simulation. Systematic effects are discussed in Sec. 4. Assuming no evidence for a signal, the 90% CL upper limit on the branching fraction, obtained from the integral $\int_0^{\mathcal{B}} \mathcal{L}_f(\mathcal{B}')d\mathcal{B}' / \int_0^{\infty} \mathcal{L}_f(\mathcal{B}')d\mathcal{B}' = 0.9$, is

$$\mathcal{B}(B^0 \to a_0^{\pm}(a_0^{\pm} \to \eta\pi^{\pm})\pi^{\mp}) < 11.5 \times 10^{-6} \ , \tag{6}$$

---

[3]From "toy" Monte Carlo studies, the difference of 1.9 events observed between the signal yields with NN and Fisher is consistent with the statistical overlap between the samples. Taking into account the 84% correlation between the signal yields of the fits with NN and Fisher, the probability to find a difference larger than that observed is 45%.
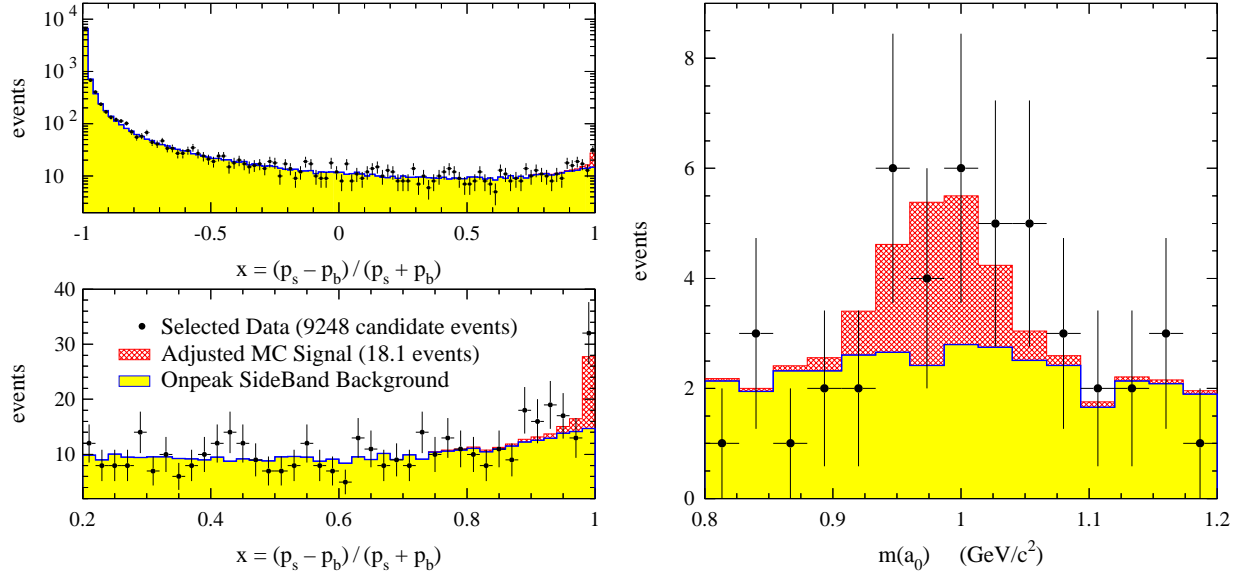
Figure 5: Left-hand plot: distributions of the x variable (7) for data (points with error bars), signal Monte Carlo (cross-hatched area) and the background expectation from on-peak sidebands (shaded area). The signal region has been expanded in the lower plot. The simulated signal contribution is normalized to the ML fit result. A signal excess is observed. Right-hand plot: projection on the $\eta\pi$ invariant mass axis after requiring $x > 0.98$, removing 44% of the signal and 99.9% of the background.

where the systematic uncertainty has been added linearly. A 65% correlation between the ML fit result (5) and the cut-based result (see Table 3) is found with a toy Monte Carlo simulation. The probability for finding a larger difference than that observed (1.6×10^{-6}) is found to be 54%.

The signal yield of the likelihood function can be displayed with the x-variable, defined by

$$ x = \frac{p_s - p_b}{p_s + p_b} \ . \tag{7} $$

Its distribution for the data sample used in the ML fit is shown by the points with error bars in the left-hand plots of Fig. 5. Also shown are the expectations from signal Monte Carlo (cross-hatched area), normalized to the signal yield of the ML fit, and background from on-peak sidebands (shaded area). A signal excess and good agreement between data and simulation are observed.

Since the information from the shape of the $\eta\pi$ invariant mass distribution is not exploited in the likelihood function, one can use projections in order to verify that the signal candidates are consistent with the a_0 hypothesis. We select events with $x > 0.98$, keeping 56% of the signal while retaining only 0.1% of the background. The distributions of the corresponding data events, as well as the signal and background expectations are shown in Fig. 5. The data are consistent with the expected enhancement at the a_0 invariant mass.

15

4 Systematic Uncertainties

The main sources of systematic uncertainty originate from the accuracy of the simulation for the reconstruction of neutrals, from the tracking efficiency and from particle identification. Dedicated studies provide estimates of these effects. A 5% uncertainty is assigned to the η reconstruction efficiency, which represents the dominant error on the selection efficiency. The tracking efficiency difference between data and Monte Carlo simulation amounts to 3.9%. An uncertainty of 1.8% is assigned due to particle identification.

Other systematics may arise from the imperfect simulation of the distributions of the discriminating variables. They have been studied with control samples. The widths and central values of the ΔE and m_{EC} signal distributions are calibrated with $B^- \to D^0(\to K^-\pi^+)\rho^-$ decays, where the estimate of systematics using final states with π^0's is expected to be conservative since the π^0's have more combinatorial background than η's. The η and a_0 invariant mass distributions have been studied with inclusive data samples. Since the line shape of the a_0 resonance is not well known [3], we have used a generous mass window (*c.f.* Sec. 3.1) so that the resulting systematic effect from the $\eta\pi$ mass requirement is small. The Fisher and NN distributions have been checked by comparing on-peak sideband data and $q\bar{q}$ Monte Carlo, where all differences are assigned as systematic errors. The uncertainty on the signal efficiency related to the limited Monte Carlo statistics is negligible.

The contamination from continuum background in the cut-based analysis is evaluated by extrapolating the number of events found in the GSB, using the known shapes of the ΔE and m_{EC} background distributions. The consistency of the parameterizations has been checked for different regions of the sidebands, and between data sidebands and $q\bar{q}$ Monte Carlo samples as well as off-peak data. Good agreement is found. Associated uncertainties are estimated by varying the shape parameters within their statistical accuracies. The same procedure has been applied to estimate the systematic uncertainties from the cuts on the event shape variables and the MVA discriminants.

The estimate of the (mostly charmless) B-background has been performed with generic charmless Monte Carlo. We expect a contamination of 0.3 events from non-resonant $\pi^+\pi^-\pi^0$ decays. The feedthrough from the unknown decay mode $B^0 \to a_0^+ K^-$ is determined from the comparison of the inclusive $a_0^+ h^-$ signal yield (*i.e.*, obtained without PID requirements) with the exclusive results of the cut-based analysis. No indication for a possible contamination from $a_0^+ K^-$ events is found. A conservative 5% systematic is assigned to the kaon fraction in the $a_0^+\pi^-$ signal.

Table 4 summarizes the relative systematic errors used for the cut-based analysis. Where they differ, uncertainties are given separately for NN and Fisher.

Systematic effects specific to the ML analysis arise from differences in the background shapes of the MVA variables between data and Monte Carlo simulation (15%). The systematic uncertainty from the correlations between the discriminating variables entering the fit, in particular those between the signal distributions of ΔE and m_{EC}, amounts to 2%. The total systematic error for the ML fit is 18%.

5 Conclusions

The preliminary analysis reported in this paper shows an excess over expected background of $B^0 \to a_0^+(980)\pi^-$ events, excluding the zero-signal hypothesis at the level of 3.7 standard deviations. Interpreted as evidence for a signal, the excess would result in the branching fraction $\mathcal{B}(B^0 \to a_0^+(a_0^+ \to \eta\pi^+)\pi^-) = (6.2\,^{+3.0}_{-2.5}\pm1.1)\times10^{-6}$, where the first error quoted is statistical and the second is systematic. This corresponds to an upper limit of $\mathcal{B}(B^0 \to a_0^+(a_0^+ \to \eta\pi^+)\pi^-) < 11.5 \times 10^{-6}$

Table 4: Summary of systematic uncertainties for the cut-based analysis.

Source	Uncertainty
η finding	5.0%
η mass and resolution	0.7%
a_0 mass and width/resolution	0.1%
Track finding	3.9%
PID	2.6%
ΔE	1.7%
m_{EC}	0.1%
θ_{T} and θ_{TP}	1.0%
MVAs	NN: 1.0%, FI: 2.0%
GSB $q\bar{q}$ background estimate	NN: 1.3 events, FI: 1.5 events
Charmless B background	0.3 events
$a_0^+ K^-$ feedthrough	5%
MC sample statistics	0.2%
B counting	1.5%
Total error on branching fraction	NN: 15.7%, FI: 17.0%

at 90% CL. We emphasize the use of improved, linear and non-linear multivariate background suppression techniques and optimal signal extraction criteria for rare decay searches.

Acknowledgements

Appendix: Cut Optimization

The cut on the MVA variable output x_{out} (the final cut being denoted $x_{\text{out}}^{\text{cut}}$) is applied following a criterion designed for rare decay searches. In particular, it does not require one to know (or guess) the branching fraction of the signal one is looking for. When searching for a rare signal, one wants

to rule out the null hypothesis[4]: "there is no signal in the data sample". For this purpose, one defines the confidence level

$$\mathrm{CL}(N, x_{\mathrm{out}}^{\mathrm{cut}}) = \sum_{n=N}^{\infty} \mathcal{P}_n(N_b) , \qquad (8)$$

where N is the number of events retained by the final cut, N_b is the expected number of background events passing the final cut, and $\mathcal{P}_n(N_b)$ is the corresponding Poisson probability distribution. If CL is below a certain threshold (*e.g.*, 5%, meaning that the hypothesis is excluded at 95% CL), one excludes the absence of rare decays, to this level. The idea is to adjust $x_{\mathrm{out}}^{\mathrm{cut}}$, hence varying both signal and background efficiencies to reach the lowest confidence level, on average.

Cut Optimization for Known Branching Fraction $\mathcal{B}$. First, if the branching fraction is known, then, for a given $x_{\mathrm{out}}^{\mathrm{cut}}$, one can predict the expected number of N_s signal events. The expected value of the CL of Eq. 8 (*i.e.*, the average over a large number of hypothetical experiments) is

$$\langle \mathrm{CL} \rangle (x_{\mathrm{out}}^{\mathrm{cut}}) = \sum_{N=0}^{\infty} \mathcal{P}_N(N_s + N_b) \, \mathrm{CL}(N, x_{\mathrm{out}}^{\mathrm{cut}}) . \qquad (9)$$

The optimal cut on x_{out}, denoted $x_{\mathrm{out}}^{\mathrm{opt}}(\mathcal{B})$, is the one which minimizes the above average, *i.e.*, which leads to the clearest rejection of the (wrong) hypothesis: "there is no signal in the data sample"

$$\langle \mathrm{CL} \rangle (x_{\mathrm{out}}^{\mathrm{opt}}(\mathcal{B})) = \langle \mathrm{CL} \rangle_{\mathrm{min}; \, x_{\mathrm{out}}^{\mathrm{cut}}} (x_{\mathrm{out}}^{\mathrm{cut}}) . \qquad (10)$$

Figure 6 (left hand plot) shows the confidence level achievable for a given number of expected signal events. Also shown are the variations of the optimal cut and the cut obtained when using the Gaussian criterion $S^2/(S + B)$ for optimization.

Cut Optimization for Unknown Branching Fraction. When no expectation for the signal branching fraction is available, Eq. 10 cannot be used to define the optimal cut value of $x_{\mathrm{out}}^{\mathrm{cut}}$. The idea is then to replace the target branching fraction by a target confidence level. One chooses a particular value for the target CL (denoted $\mathrm{CL}^{\mathrm{cut}}$) one is aiming at to define the optimal $x_{\mathrm{out}}^{\mathrm{cut}}$ value as the value $x_{\mathrm{out}}^{\mathrm{opt}}$ (now without $(\mathcal{B})$ as an argument) for which the equality

$$\langle \mathrm{CL} \rangle (x_{\mathrm{out}}^{\mathrm{opt}}) = \mathrm{CL}^{\mathrm{cut}} , \qquad (11)$$

is reached for the smallest $\mathcal{B}$. In the following we use $\mathrm{CL}^{\mathrm{cut}} = 0.05$. The performance for unknown branching fraction is illustrated for the NN discriminant in the right hand plot of Fig. 6.

References

[1] A.S. Dighe, C.S. Kim , *Phys.Rev.D***62**, 111302 (2000).

[2] S. Laplace and V. Shelkov, "*CP Violation and the Absence of Second Class Currents in Charmless B Decays*", LAL 01-24, LBNL-47757, hep-ph/0105252 (2001), to appear in Eur. Phys. J. C.

---

[4]It can be shown that ruling out the opposite hypothesis "there is signal in the data sample", leads to an identical prescription.
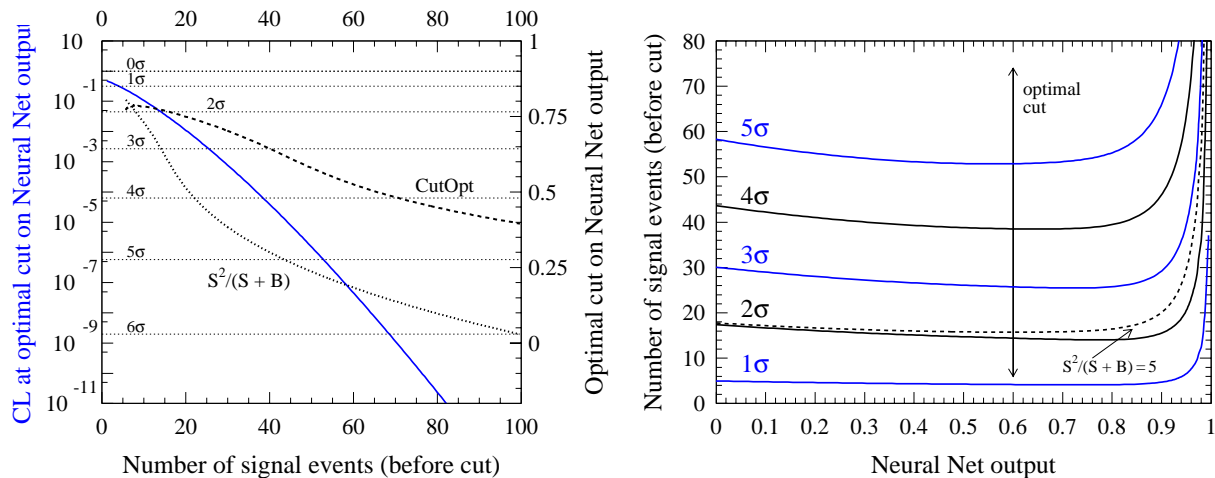
Figure 6: Left-hand plot: expected confidence levels and optimal cuts on the NN discriminant for an analysis where the branching fraction is known. The solid line gives the confidence level, obtained when using the optimal cut, as a function of the number of signal events (before cut). The dashed line is the optimal cut for a given number of events, and the dotted line gives the optimal cut using the criterion $S^2/(S+B)$. Right-hand plot: average number of signal events before NN cut, needed in the data sample to attain a given confidence level, on the average. Shown are the curves corresponding to $1\ldots5\sigma$. The minima of the curves correspond to the optimal cuts at a given significance level. Notice that the optimal cuts are approximately independent of the branching fraction. Shown in addition is the curve obtained for the constant signal excess $S^2/(S+B) = 5$, corresponding to a significance of 2 standard deviations.

[3] Particle Data Group, D.E. Groom *et al.*, Eur. Phys. Jour. C **15**, 1 (2000).

[4] *BABAR* Collaboration, B. Aubert *et al.*, *"The BABAR Detector"*, hep-ex/0105044 (2001), to appear in Nucl. Instr. and Meth..

[5] P. Gay, B. Michel, J. Proriol, and O. Deschamps, *"Tagging Higgs Bosons in Hadronic LEP-2 Events with Neural Networks."*, In Pisa 1995, New computing techniques in physics research, 725 (1995).

[6] *BABAR* Collaboration, P.F. Harrison and H.R. Quinn, eds., *"The BABAR Physics Book"*, SLAC-R-504 (1998).

[7] CLEO Collaboration, D.M. Asner *et al.*, *Phys. Rev.* **D53**, 1039 (1996).

[8] ARGUS Collaboration, H. Albrecht *et al.*, *Phys. Lett.* **B185**, 218 (1987); **B241**, 278 (1990).